ENVIRONMENTAL RESEARCH
LETTERS

PURPOSE-LED PUBLISHING™

Celebrating the 20th anniversary of Environmental Research Letters

LETTER • OPEN ACCESS

Satellite-detected nitrogen oxides emission changes from power plant dynamics in North China

To cite this article: Chenghao Xu *et al* 2026 *Environ. Res. Lett.* **21** 154012

ENVIRONMENTAL RESEARCH
LETTERS

OPEN ACCESS

RECEIVED
30 March 2026

REVISED
24 June 2026

ACCEPTED FOR PUBLICATION
3 July 2026

PUBLISHED
30 July 2026

LETTER

Satellite-detected nitrogen oxides emission changes from power plant dynamics in North China

Chenghao Xu[1], Jintai Lin[1,2,*], Sijie Wang[1], Hao Kong[1], Yuhang Zhang[1], Yang Yun[1], Fangxuan Ren[1], Mengying Wang[1], Wanshan Tan[1], Jianxiao Wang[3,4], Lei Bai[5] and Jian Gao[6]

[1] Laboratory for Climate and Ocean-Atmosphere Studies, Department of Atmospheric and Oceanic Sciences, School of Physics, Peking University, Beijing 100871, People's Republic of China
[2] Institute of Carbon Neutrality, Peking University, Beijing 100871, People's Republic of China
[3] National Engineering Laboratory for Big Data Analysis and Applications, Peking University, Beijing 100871, People's Republic of China
[4] Peking University Ordos Research Institute of Energy, Ordos 017000, People's Republic of China
[5] Shanghai Artificial Intelligence Laboratory, Shanghai 200232, People's Republic of China
[6] State Key Laboratory of Environmental Criteria and Risk Assessment,Chinese Research Academy of Environmental Sciences, Beijing 100012, People's Republic of China
[*] Author to whom any correspondence should be addressed.

E-mail: linjt@pku.edu.cn

Keywords: nitrogen oxides, satellite, coal-fired power plants, emissions

Supplementary material for this article is available online

Abstract

Emissions of nitrogen oxides (NO_x) from coal-fired power plants (CFPPs) pose a significant challenge to air quality. In China, although policies like 'Promoting the Big and Quashing the Small' and the adoption of ultra-low emission (ULE) technologies have been implemented in power plants, accurately quantifying their impacts on NO_x emissions remains difficult due to lack of facility-specific information. This study investigates the influence of CFPP changes on NO_x emissions from 2018 to 2024 in North China, by integrating a self-compiled, high-accuracy power plant database (with 517 plants in North China, including 109 retired or newly built) with satellite-derived NO_x emission data at a high spatial resolution ($0.05° \times 0.05°$). We find that among the locations with no industrial sources, emissions show substantial reductions (-1.97 kg km^{-2} h^{-1} on average; Wilcoxon test $p < 0.001$; t-test $p < 0.001$) where CFPPs were retired during this period, compared with the increases ($+0.76$ kg km^{-2} h^{-1} on average; Wilcoxon test $p < 0.01$; t-test $p < 0.01$) where CFPPs equipped with ULE technology were newly built. However, when the retired or newly built CFPPs are located in the same $0.05° \times 0.05°$ grid cells with industrial sources, their emission signals are often dominated by industrial emission reductions, resulting in emission declines in both cases. These results underscore the rising relative contribution of industrial emissions in regions where power plants and heavy industry are spatially co-located, and highlight the need to strengthen emission monitoring and control efforts directed at the industrial sector. By comparison, existing emission inventories have difficulty in capturing the power plant dynamics, particularly the effect of CFPP retirement. Our results demonstrate the value of satellite remote sensing coupled with detailed facility information for assessing point-source emission dynamics.

1. Introduction

Nitrogen oxides (NO_x) are critical atmospheric pollutants affecting air quality and human health (Seinfeld *et al* 1998, Hoek *et al* 2013). They are key precursors of ground-level ozone (O_3) and secondary fine particulate matter ($PM_{2.5}$), driving heavy pollution events and associated public health risks (Murray *et al* 2020). North China, encompassing Beijing, Tianjin, Hebei, Shanxi, and Inner Mongolia, has long been a leading region for energy production and a hotspot for atmospheric pollution (Fan *et al* 2020, Zhu *et al* 2022, National Bureau of Statistics of China 2024). In this region, the concentration of coal-fired power plants

(CFPPs) and other heavy industries makes it a primary focus for NO_x emission control (State Council of China 2013, 2017).

The power sector, particularly CFPPs, has historically been a dominant contributor of China's NO_x emission (Liu *et al* 2015, Tong *et al* 2018). Recognizing the severity of the issue, the Chinese government has implemented a series of stringent policies targeting this sector over the past decades. Two of the most pivotal measures are the 'Promoting the Big and Quashing the Small' policy, which replaces small, inefficient units with larger, more efficient ones, and the nationwide promotion of ultra-low emissions (ULE) technologies. The ULE technologies limit the emissions of NO_x, sulfur dioxide (SO_2), and particulate matter to levels comparable to or lower than those of uncontrolled gas-fired plants (National Development and Reform Commission 2014); note that gas-fired plants equipped with selective catalytic reduction can achieve substantially lower NO_x emission concentrations. The effectiveness of power-sector emission control policies has been assessed through approaches such as bottom–up emission inventories and the continuous emissions monitoring systems (CEMS) network (Liu *et al* 2015, Tong *et al* 2018, Zheng *et al* 2018, Tang *et al* 2019). However, emission inventories face temporal lags in statistical data collection and are unable to capture facility-level operational changes in a timely manner (Li *et al* 2017, Liu *et al* 2019b), while CEMS data remain inaccessible to the public. These limitations motivate the need for a timely, accessible, and spatially resolved approach to quantify the impacts of individual power plant dynamics on NO_x emissions.

Satellite remote sensing complements ground-based measurements and emission inventories, offering a timely and objective method to track atmospheric composition changes (Li and Wang 2019, Xu *et al* 2023, Kong *et al* 2025). Sensors such as the ozone monitoring instrument and the TROPOspheric ozone monitoring instrument (TROPOMI) have been extensively used to estimate NO_x emission changes over China (Liu *et al* 2017, Yan *et al* 2023, Kong *et al* 2025, Lu *et al* 2025).

Given the limitations of satellite data, their applications to track power plant emissions require precise, independent ground truth information about the operational status of power plants. Previous work has largely relied on publicly available power plant databases (Wang *et al* 2023, Yan *et al* 2023, Liu *et al* 2024, Zeng *et al* 2025). However, these databases are often subject to inaccurate geolocation information, lack of data on small- and medium-sized power plants, and/or lack of critical operational details to facilitate emission assessment. To address this research gap, this study leverages a novel, integrated approach that combines a self-compiled, high-accuracy power plant database with satellite-derived high-resolution NO_x emission data over North China in summers (June–August) of 2018–2024. First, we establish a comprehensive thermal power plant database for China by synthesizing existing datasets and multi-source geographic information. Our database includes key attributes such as power generation capacity and precise geolocation. For the 517 plants in North China, we further refine the operational timelines (i.e. start and retirement dates) since 2018 by analyzing multi-temporal satellite imagery and multiple lines of industrial reports. Then, NO_x emission data retrieved at a $0.05° \times 0.05°$ resolution from the TROPOMI satellite instrument are used to evaluate the capability of satellite observations in detecting emissions from individual CFPPs. Finally, we investigate the emission characteristics of newly built and retired power plants, as well as the potential interference from surrounding industrial activities on the power plant signals. Beyond its methodological contribution, this study sheds light on how stringent emission controls in the power sector leads to a broad shift from power-sector-crucial to more industrial-sector-driven NO_x emission burden in North China.

2. Methods

2.1. China power facility database (CPFD)

We build a CPFD with over 3400 power facilities (including more than 2500 plants burning coal and others burning biomass or waste) in China from 2013 to 2024, including 517 plants in North China. For North China, the database includes precise location, capacity, surrounding environment information, and operational timelines such as start and retirement dates for each power plant.

We first adopt a 2013 power facility database from Environmental Statistics, which covers plants of all sizes but suffers from inaccurate geolocation information. For facilities built after 2013, we use the global energy monitor (GEM) database for supplementation and cross-verification, updating the list of power-generating units to 2024. The GEM data contain information on capacity and commissioning dates but not electricity generation.

We then perform geolocation calibration for all facilities. We use the AMAP point of interest search, which locates approximately 60% of facilities; the remaining 40% are resolved using business registration addresses, news searches, and Google Earth imagery. Through this process, we obtain specific geolocations for all power facilities. We further refine the location accuracy using Google Earth historical imagery and the World Imagery Wayback service. This correction ensures that the accuracy of each plant's geo-coordinates is at the hundred-meter level. For plants near grid-cell boundaries, spatial assignment is cross-checked against the surrounding 11×11 grid cells in terms of NO_x emission and

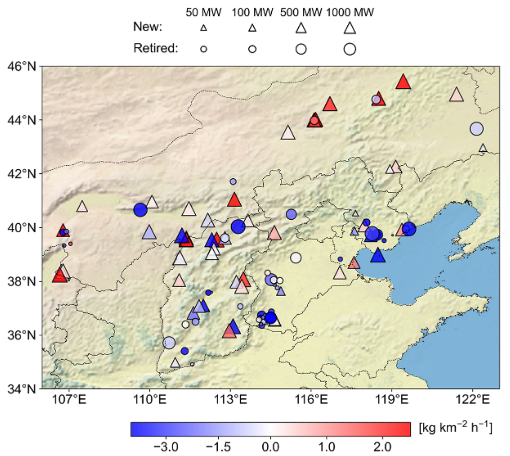

Figure 1. Distribution of retired and newly built power plants in North China from 2018 to 2024. Circles represent retired plants, and triangles represent newly built plants. Shape size indicates plant capacity, while color denotes the change in de-backgrounded NO_x emission (average emission after plant start/retirement date minus average emission before plant start/retirement date) at each grid cell.

NO_2 vertical column densities (VCD) distributions; no systematic misassignment is identified. Grid cells are classified as industry-influenced if multi-temporal Google Earth and World Imagery Wayback imagery confirm the presence of high-NO_x industrial facilities (steel mills, cement plants, chemical complexes, or coking facilities) within the $0.05° \times 0.05°$ domain.

For North China, we further collect operational status changes for each power facility. We determine retirement dates through government announcements combined with satellite historical imagery. For newly built units, we obtain precise commissioning dates from industrial news sources. The locations of these power facilities are shown in figure 1.

2.2. NO_x data from satellite and bottom-up inventories

We use tropospheric NO_2 VCDs and associated top-down NO_x emission data to assess the impacts of power plant changes. The NO_2 VCD data are taken from the POMINO-TROPOMI v1.2.2 product (Liu *et al* 2020). POMINO adopts the tropospheric slant column densities of NO_2 from the operational product, and re-calculates the air mass factors and effective cloud fractions to derive the VCDs. Compared to the operational algorithm, POMINO algorithm explicitly accounts for the effects of aerosols and surface reflectance anisotropy and adopts higher-resolution (25 km versus 100 km) *a priori* NO_2 vertical profiles. This results in a lower bias and better coverage of NO_2 data, especially at polluted situations (Liu *et al* 2019a, 2020, Zhang *et al* 2022, Zhang *et al* 2025).

The top–down NO_x emissions are estimated based on the POMINO-TROPOMI v1.2.2 NO_2 VCD data, using an updated version of the PHLET (Peking University High-Resolution Lifetime-Emission-Transport) inversion method (Kong *et al* 2022, 2025). The update refers to the adoption of wind data from the real-time ECMWF analysis (0.09° lon. × 0.09° lat., Hersbach *et al* (2020)) vertically averaged over 0–500 m above the surface as a common practice (Liu *et al* 2016, 2017, Beirle *et al* 2019) in place of previously-used GEOS-FP (0.3125° lon. ×0.25° lat.) to greatly improve the accuracy of PHLET-simulated horizontal transport of NO_x. We apply the updated PHLET inversion method in China to derive surface NO_x emissions at a horizontal resolution of $0.05° \times 0.05°$ for each summer (June–August) from 2018 to 2024.

To focus on anthropogenic emissions, we remove contributions from natural sources including soil and open fire. The hourly soil NO_x emissions are taken from Weng *et al* (2020) and daily open fire emissions from the Global Fire Assimilation System (Kaiser *et al* (2012)), with the interannual variability from 2018 to 2024 accounted for. Detailed derivation of PHLET emission inversion and associated uncertainties is shown in Kong *et al* (2022). Emissions are expressed based on the molecular weight of NO_2 (46 g mole^{-1}), and emission uncertainties are expressed as one standard deviation error. The resulting emission data include the contributions from all anthropogenic sources. As such, at the grid-cell level, emissions from power plants may be mixed with other sources within the same grid cell such as industry, transportation and residential use. Therefore, we perform a de-background procedure for emissions in all grid cells containing power plants. Specifically, for each grid cell containing power plants, we remove as background the 25th percentile of emissions and VCDs from the surrounding 11×11 grid cells (excluding that grid cell with power plants). The embedded assumption is that the contribution from all non-power-plant sources can be approximated by this background value. However, this procedure cannot fully remove the contribution from other co-located sources. Given the large influences of co-located industrial sources, we will analyze the power plant emission changes under industry-influenced and non-industry-influenced situations separately; and other non-industrial interfering sources will be discussed when relevant. We test other percentile values (10th and 50th) for background subtraction and find little impact on the conclusion regarding the emission changes driven by power plant retirement and establishment. Pre- and post-event NO_x emission changes are tested using both a one-sample Wilcoxon signed-rank test (a non-parametric test on whether the median value = 0) and a one-sample t-test (a parametric test on whether the mean value = 0), with two-tailed tests applied throughout.

Additionally, to examine how power plant changes are reflected in the existing emission datasets, we utilize two bottom-up inventories, including the

MEIC (Multi-scale Emissions Inventory of China; www.meicmodel.org, last access: 22 January 2026) v2.0 inventory in China (Liu *et al* 2015, Li *et al* 2017, Tong *et al* 2018) and the CEDS (Community Emissions Data System v_2025_04_18) inventory (Hoesly *et al* 2025). Both emission inventories are available through 2023. The spatial resolution of CEDS is 0.1° × 0.1°, while MEIC has a spatial resolution of 0.25°. For each inventory, we calculate the summer (June, July and August) mean emissions to match the PHLET dataset.

3. Results

3.1. Changes in power plants in North China

Figure 2 illustrates a significant increasing trend in thermal power generation across North China from 2018 to 2024, characterized by a distinct spatial shift in energy production. During the summer peak seasons, total thermal power generation in North China region rose by 30.2%. This growth was unevenly distributed: while the Beijing–Tianjin–Hebei (BTH) region saw a negligible increase of 2.9%, Shanxi and Inner Mongolia experienced substantial surges of 29.4% and 57.9%, respectively. Consequently, Inner Mongolia has replaced BTH as the primary energy hub, now contributing over 45% of the thermal power output in North China.

However, this surge in power generation has not translated into a proportional rise in satellite-derived NO_x emissions. Summertime de-backgrounded NO_x emissions at the grid cells with power plants in BTH and Shanxi decreased by 52.9% and 34.6%, respectively, with only Inner Mongolia showing a slight increase (17.6%). Here, all power plants (retired, newly built, or in continuous operation during 2018–2024) are considered. These results are consistent with the adoption of ULE technologies, the declining share of coal-fired power, changes in plant operating status, and interference from industrial sources within the same grid cells. The observational design of this study does not permit strict causal attribution or quantitative partitioning of the individual roles of these contributing factors. Our subsequent analysis therefore focuses on these 109 CFPPs retired or built during 2018–2024 (detailed information in supplementary table 1).

Between 2018 and 2024, 50 power plants were retired in North China (figure 1). Most of them are concentrated in Hebei Province, and over half of them are small-scale facilities with capacity under 100 MW. This reflects Hebei's strict coal-fired power optimization targets during the study period (https://hbdrc.hebei.gov.cn/xxgk_2232/fdzdgknr/ghjh/gh/202309/t20230907_87223.html, Last accessed: 10 August 2025) requiring a reduction in the proportion of coal-fired power generation capacity while decreasing the share of small (⩽200 MW) units within CFPPs. Conversely, 59 power plants were newly built during this period, mainly in Shanxi and Inner Mongolia. Among them, 49 were large plants with more than 500 MW in capacity; particular in Inner Mongolia, over half of the newly built plants were ultra-large facilities exceeding 1000 MW in capacity. This aligns with the policy objectives outlined in the Inner Mongolia Energy Development Plan (www.nmg.gov.cn/zwgk/zfxxgk/zfxxgkml/ghxx/zxgh/202012/t20201208_312918.html, Last access: 10 February 2026). Overall, power plant changes in North China in recent years have adhered to the 'Promoting the Big and Quashing the Small' policy, with extensive closures of small and outdated plants and a shift of generation centers to Inner Mongolia and Shanxi.

3.2. NO_x emissions in response to power plant dynamics

As shown in figure 3, grid cells with retired power plants show a consistent downward trend in both NO_x emissions and NO_2 VCDs from 2018 to 2024, while those with newly built plants exhibit a more stable or slightly increasing trajectory despite the substantial capacity additions.

However, figure 3 also highlights a substantial variability of emissions across grid cells with retired or newly built power plants, as indicated by the wide interquartile ranges (IQR) and extended whiskers. This heterogeneity implies that the satellite-detected emission signal at a given 0.05° × 0.05° grid cell is not solely driven by the power plants themselves but is likely modulated by other co-located emission sources. Specifically, the presence of co-located industrial facilities may mask or amplify the emission signals. To address this, we further classify and analyze the grid cells based on the presence of industrial interference. We use Google Earth and World Imagery Wayback to manually check whether a power plant is co-located with and thus influenced by industrial facilities in the associated grid cell.

There are 52 power plants located in non-industry-influenced grid cells, with 31 newly built plants and 21 retired plants. Among these 52 plants, the changes in power plant operational status are effectively captured by satellite-derived emissions. Most newly built power plants in non-industry-influenced grid cells exhibit statistically significant emission increases (+0.76 kg km^{-2} h^{-1} on average; Wilcoxon $W = 62$, $p < 0.001$; $t = 4.01$, $p < 0.001$). The magnitude is small and de-backgrounded emissions after commissioning remain low (<5 kg km^{-2} h^{-1}), consistent with effective NO_x control through ULE technology. Solar-driven suppression of midday thermal output could reduce captured emissions by up to ∼20% in 2024, but this does not introduce a directional bias between plant categories (section S1).

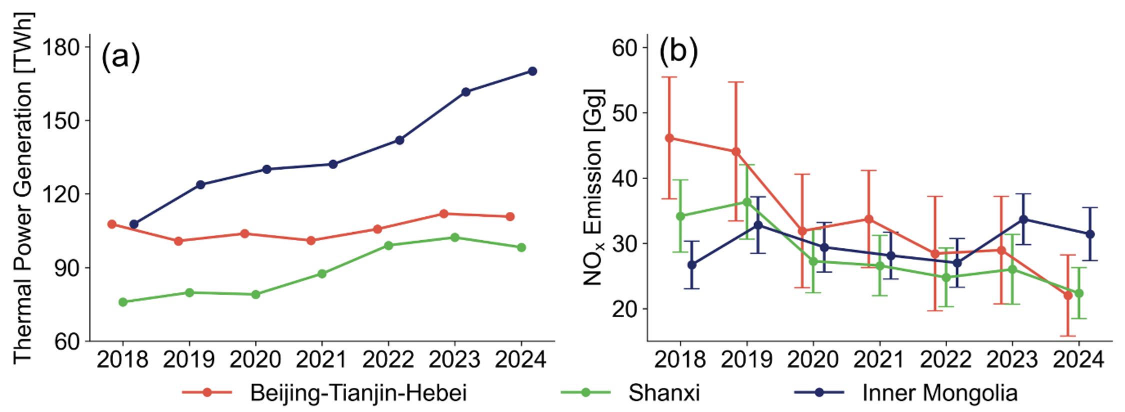

Figure 2. Summertime thermal power generation and NO_x emissions in North China from 2018 to 2024. (a) Thermal power generation in the Beijing–Tianjin–Hebei region, Shanxi Province, and Inner Mongolia Autonomous Region. (b) De-backgrounded NO_x emissions at the grid cells with power plants in these regions, with error bars representing 1-σ uncertainties.

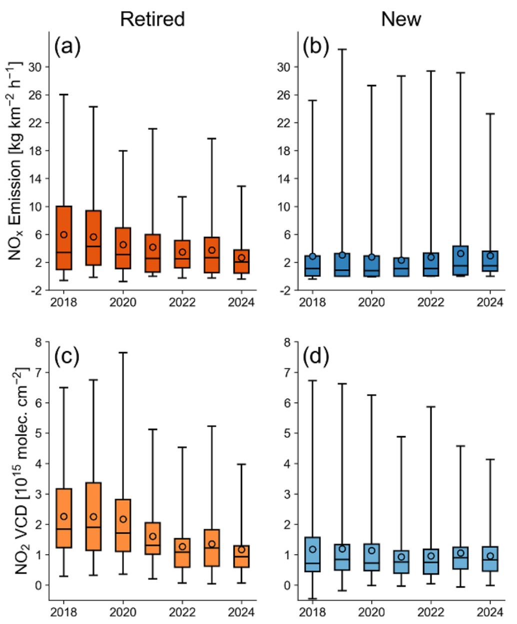

Figure 3. Summertime NO_x emissions and NO_2 VCDs at the grid cells with retired or newly built power plants in North China from 2018 to 2024. (a) De-backgrounded NO_x emissions at the grid cells with retired power plants, (b) De-backgrounded NO_x emissions at the grid cells with newly built power plants, (c) De-backgrounded NO_2 VCDs at the grid cells with retired power plants, (d) De-backgrounded NO_2 VCDs at the grid cells with newly built power plants. The box bounds the IQR divided by the median, and Tukey-style whiskers extend to the maximum and minimum values. Circles represent the average value.

To further examine the effect of newly built power plants, we present more details for a few representative plants (see their IDs in figure 4(a)). For Power Plant No. 43 (figure S1), satellite imagery shows that the facility was still not under construction in 2019. Subsequently, its two units commenced operations in July and November 2023, respectively. Comparing the spatial distributions before and after these dates for NO_2 VCDs and NO_x emissions reveals a distinct point-source signal from this power plant. Specifically, both the VCDs and emissions show substantial increases in 2024. In contrast, there are several cases in figure 4(a) where emissions decreased despite the establishment of new power plants, with an outstanding example being Power Plant No. 53 (figure S2). This facility was a Phase II expansion project located in an urban area; thus the emission reduction signals from Phase I power generation units and other anthropogenic sources within the grid cell likely outweigh the additional emissions from the new units, resulting in an overall decline.

For non-industry-influenced retired plant grid cells ($n = 19$), both tests confirm significantly negative emission changes (-1.97 kg km^{-2} h^{-1} on average; Wilcoxon $W = 35$, $p < 0.01$; $t = -3.07$, $p < 0.01$), confirming that the visual pattern in figure 3 reflects a genuine and robust emission reduction following plant retirement. The emissions greatly differ across these grid cells especially before the power plants were retired, likely reflecting the substantial cross-plant differences in emission control technology in earlier years. Despite having smaller capacities than newly built plants, retired plants showed notably higher pre-retirement emissions, owing to their older age and lack of advanced emission control technologies. Missions in non-industry-influenced grid cells did not drop to zero following power plant retirement (figure 4(c)). This is primarily because these older plants are often situated in urban centers, where dense residential areas, traffic, or other sources lead to NO_x emissions. Although legacy plants may exhibit midday peaking behavior that could overestimate pre-retirement emissions at TROPOMI overpass time, the directional conclusion remains valid under bounding-scenario analysis (section S1).

We further present a few exemplary retired power plants for detailed analyses. For Power Plant No. 104 (figure S3), satellite imagery indicates that this

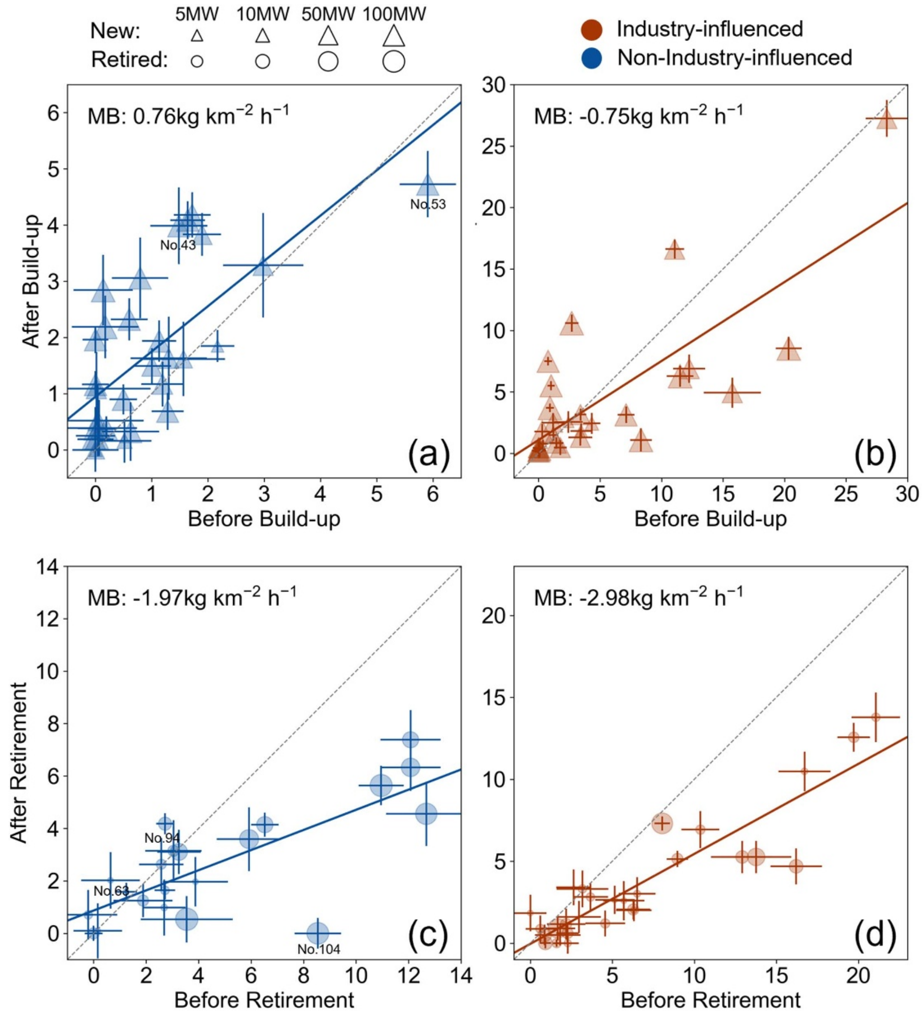

Figure 4. Scatter plot for average de-backgrounded NO_x emissions before and after power plant operational changes. Power plants were newly built or retired during 2018–2024. Emission changes are expressed in kg km^{-2} h^{-1}. The horizontal and vertical lines surrounding the points represent the 1-σ uncertainty before and after their build-up/retirement, respectively. The solid line represents the fitted line for the scatter points in each panel. The IDs of several representative power plants are marked in the scatter plot. (a) Changes of de-backgrounded emissions in non-industry-influenced grid cells containing newly built power plants. (b) Changes of de-backgrounded emissions in industry-influenced grid cells containing newly built power plants. (c) Changes of de-backgrounded emissions in non-industry-influenced grid cells containing retired power plants. (d) Changes of de-backgrounded emissions in industry-influenced grid cells containing retired power plants.

plant was still operational in 2018 but had been completely shut down by 2025. The government mandated its transition to emergency reserve status by the end of 2023. Both the NO_2 VCDs and NO_x emissions at the grid cell where the plant was located show a significant decrease. In contrast, there are a few cases in figure 4(c) where emissions increased in certain grid cells despite power plant retirements, with the most outstanding being Power Plant No. 63 and No. 94. As shown in figure S4, the grid cell containing the retired Plant No. 94 (86 MW) hosts two other newly built larger power plants (No. 30: 1320 MW and No. 48: 700 MW), which dominate the emission signal. For Plant No. 63 (figure S5), the reduction signal from its retirement was likely masked by variations in transportation-related emissions, given its small capacity (12 MW) and urban location.

Among the non-industry-influenced grid cells (figure 5), those with retired power plants exhibit a positive correlation between pre-retirement emissions and power generation capacities, despite the existence of data scatter. In contrast, those grid cells with newly built power plants exhibit little correlation between emissions and capacities. At a given capacity level, grid cells with retired plants exhibit much higher pre-retirement emissions than those with newly built plants. Additionally, according to data from the China Electricity Council (Obtained from www.ceicdata.com/zh-hans/china/utilization-of-power-generating-equipment, Last access: 19 June 2026), provincial average utilization hours of thermal power equipment in Inner Mongolia and Shanxi, regions that absorbed the bulk of newly built capacity, declined only modestly over 2018–2024, by 7.3% and 2.3%, respectively. By contrast, in Hebei Province,

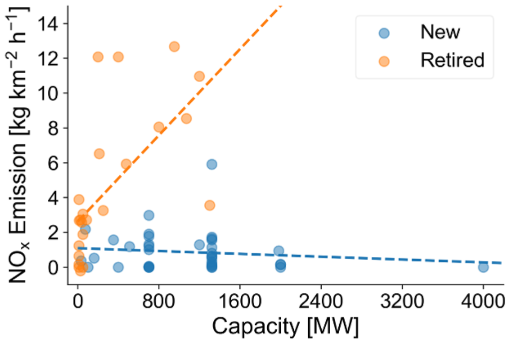

Figure 5. Scatter plot of average de-backgrounded NO_x emissions versus installed capacity in non-industry-influenced grid cells. The de-backgrounded emissions of newly built power plants represent the average of summer emissions in all years since build-up in the corresponding grid cells. The de-backgrounded emissions of retired power plants reflect the average of summer emissions prior to the year of retirement in the corresponding grid cells. The data period spans from 2018 to 2024. The figure compares de-backgrounded emission levels; emission intensity per unit of electricity generated cannot be derived from the data as presented, given the absence of facility-level generation records. Regression lines are shown for visual reference.

where most plant retirements occurred, average utilization hours declined by 22.7% over the same period. This pattern is consistent with retired legacy units having progressively lower utilization rates, while newly built ULE units maintained higher utilization, an aggregate configuration that further supports the conclusion that structural improvements in emission factors, rather than reduced operational output, are the dominant driver of the observed de-backgrounded NO_x emissions declines at the grid cells with power plants in North China.

There are 57 power plants co-located with industrial facilities, among which 28 are newly built and 29 are retired. For these 57 plants, the changes of de-backgrounded emissions at the corresponding grid cells are more heterogeneous for both newly built and retired power plants (figures 4(b) and (d)). Here, the grid cells with newly built power plants show an average de-backgrounded emission change of -0.75 kg km^{-2} h^{-1} (Wilcoxon $W = 178$, $p = 0.58$; $t = -0.88$, $p = 0.39$), with many grid cells exhibiting emission declines. This reflects a ‘masking effect’: the emission signals of newly built plants are overwhelmed by stronger industrial emissions, which are themselves declining under strict emission controls (State Council of China 2017), masking the power plant signal. For the grid cells with retired power plants and industrial influence, de-backgrounded NO_x emissions show substantial reductions with an average of -2.98 kg km^{-2} h^{-1}, a much larger drop than in the counterpart case for non-industry-influenced grid cells (-1.97 kg km^{-2} h^{-1} on average; Wilcoxon $W = 22$, $p < 0.001$; $t = -5.14$, $p < 0.001$). This reflects the combined result of closing the power plants and reducing co-located industrial emissions.

To examine whether satellite-derived emissions provide information beyond traditional inventories, we compare with CEDS v2025_04_18 and MEIC v2.0 (both available through 2023), analyzing power-sector NOx changes in grid cells of plants that changed status during 2018–2023 (figure 6). We find that CEDS captures emission change signals from newly built plants (with an average emission increase of 2.40 kg km^{-2} h^{-1}), likely due to its integration of the GEM database for new units; however, it fails to reflect the emission reductions from retired plants (with an average emission change of $+0.02$ kg km^{-2} h^{-1}). The MEIC inventory exhibits negligible emission responses to both new ($+0.02$ kg km^{-2} h^{-1}) and retired (-0.03 kg km^{-2} h^{-1}) plants, suggesting a lack of timely adjustments for these facility-level dynamics. These results underscore the unique advantage of satellite-based emissions in properly tracking point-source dynamics.

4. Conclusion and outlook

This study evaluates the impacts of structural dynamics in CFPPs on NO_x emissions in North China from 2018 to 2024. By integrating a self-compiled power plant database with satellite-derived high-resolution emissions, we quantify the environmental effectiveness of the ‘Promoting the Big and Quashing the Small’ under ULE implementation, demonstrating that satellite remote sensing augmented with facility information can effectively capture point-source emission dynamics.

The retirement and establishment of power plants led to opposite emission changes in the grid cells with no industrial interference. The retirement of older, smaller units, which often lack advanced pollution control facilities, resulted in substantial reductions of emissions (1.97 kg km^{-2} h^{-1} on average). Conversely, despite the large capacity of newly built power plants, their emission impacts were small with an average increase by 0.76 kg km^{-2} h^{-1}, consistent with the adoption of ULE technology. In non-industry-influenced grid cells that contain newly built

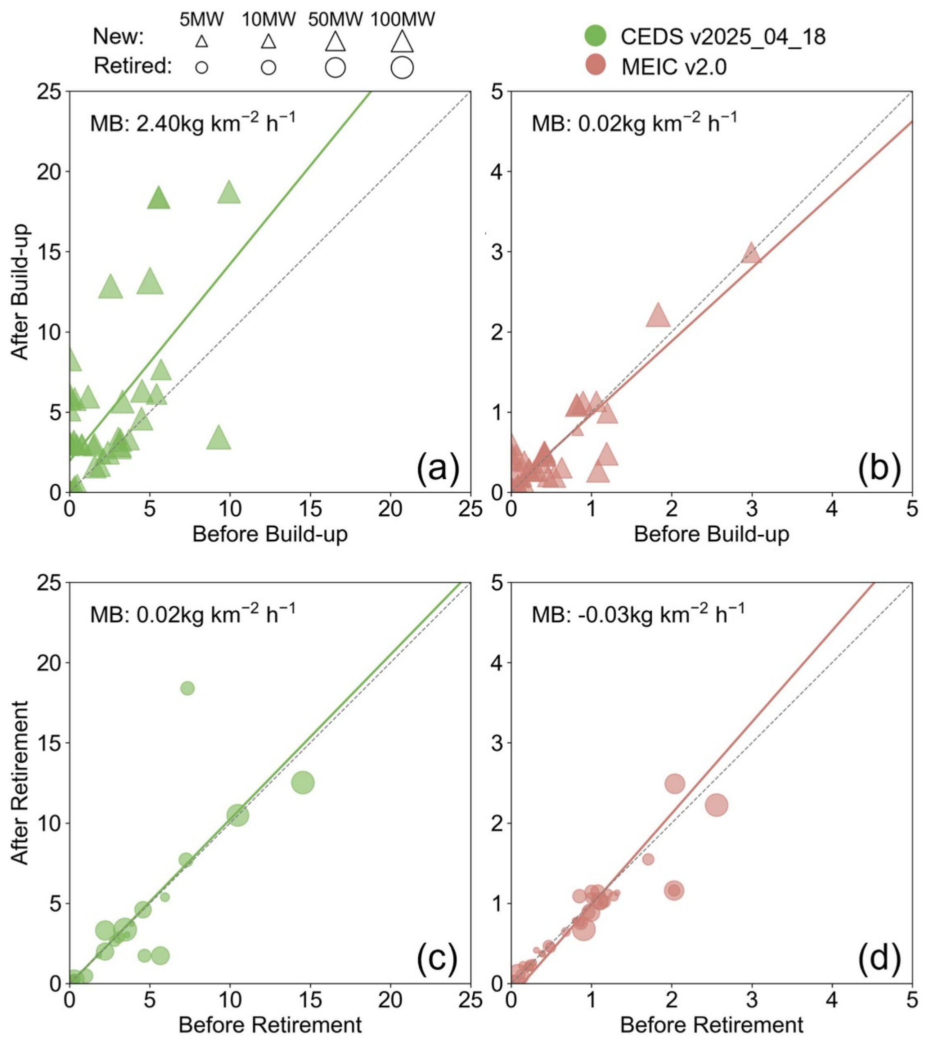

Figure 6. Scatter plot for average NO_x emissions in bottom-up inventories before and after power plant operational changes. Power plants were newly built or retired during 2018–2023. Emission changes are expressed in kg km^{-2} h^{-1}. The solid line represents the fitted line for the scatter points in each panel. (a) Emission changes in CEDS v2025_04_18 grid cells containing newly built power plants. (b) Emission changes in MEIC v2.0 grid cells containing newly built power plants. (c) Emission changes in CEDS v2025_04_18 grid cells containing retired power plants. (d) Emission changes in MEIC v2.0 grid cells containing retired power plants.

or retired CFPPs, satellite-derived NO_x emissions from ULE-equipped plants are substantially lower than those from retired legacy plants at comparable capacity levels, which suggests that coal-fired power plays a much smaller role in local NO_x emissions over the past few years. A comprehensive sectoral decomposition of total NO_x emissions across North China is beyond the scope of this study, which focuses on grid cells containing power plants that changed operational status between 2018 and 2024.

We also identify a 'masking effect' where industrial emissions dominate co-located power plant signals, decoupling grid-cell emission changes from power plant dynamics. This shift in sectoral contributions necessitates greater focus on industrial sources, challenging non-sector-specific inversions and ground-based monitoring networks. Clearly, the industrial sector should be a primary target in future emission control efforts. In particular, policy instruments, monitoring systems, and accountability mechanisms that were historically designed around CFPPs could be adapted to track and regulate more heterogeneous industrial point sources. In this sense, the power sector's rapid adoption of ultra-low-emission technology can be viewed as one stage of environmental modernization, after which further progress in NO_x reduction will increasingly depend on more complex and decentralized industrial emission controls.

Future work is warranted to further refine the assessment of point-source emissions. The isolation of point-source signals in high-background-value locations remains a challenge. Integrating chemical transport models, artificial intelligence algorithms and big Earth data will help resolve the complex interference from surrounding emission sources. Additionally, satellite data from TROPOMI are still imperfect in spatial resolution (~5 km), and, as a polar-orbit instrument, with a ~13:30 local overpass, TROPOMI cannot capture intraday emission variability (section S1). Integration of geostationary satellite data will enable hourly constraints and help disentangle daytime solar generation effects on fossil-fuel plant operation.

The precise geolocations and operational timelines in the CPFD provide facility-level anchors for a range of future applications. For example, when combined with relevant satellite retrievals, the database can support multi-pollutant studies of SO_2 and particulate matter, as well as facility-level CO_2 emission tracking in support of China's national carbon market.

Acknowledgments

This research is supported by the National Natural Science Foundation of China (Grant No. 42430603), the National Key Research and Development Program of China (Grant No. 2023YFC3705802) and the China Postdoctoral Science Foundation (grant no. 2025T180079 & 2024M760087). We thank for the technical support of the National Large Scientific and Technological Infrastructure "Earth System Numerical Simulation Facility" (https://cstr.cn/31134.02.EL).

Data availability statement

The data cannot be made publicly available upon publication due to legal restrictions preventing unrestricted public distribution. The data that support the findings of this study are available upon reasonable request from the authors.

Supplementary Information available at https://doi.org/10.1088/1748-9326/ae860b/data1.

Supplementary Table available at https://doi.org/10.1088/1748-9326/ae860b/data2.

ORCID iDs

Chenghao Xu 0000-0003-0055-2318
Jintai Lin 0000-0002-2362-2940
Sijie Wang 0009-0007-5688-1993
Hao Kong 0000-0001-5038-2914
Fangxuan Ren 0000-0003-4082-8358

References

Beirle S, Borger C, Dörner S, Li A, Hu Z, Liu F and Wagner T 2019 Pinpointing nitrogen oxide emissions from space *Sci. Adv.* **5** eaax9800

Fan H, Zhao C F and Yang Y 2020 K.: a comprehensive analysis of the spatio-temporal variation of urban air pollution in China during *Atmos. Environ.* **220** 2014–8

Hersbach H *et al* 2020 The ERA5 global reanalysis *Q. J. R. Meteorol. Soc.* **146** 1999–2049

Hoek G, Krishnan R M, Beelen R, Peters A, Ostro B, Brunekreef B and Kaufman J D 2013 Long-term air pollution exposure and cardio- respiratory mortality: a review *Environ. Health* **12** 43

Hoesly R, Smith S, Ahsan H, Prime N, O'Rourke P, Crippa M and Wang S 2025 CEDS v_2025_04_18 emission data (April-18-2025) (https://doi.org/10.5281/zenodo.15127477)

Kaiser J W *et al* 2012 Biomass burning emissions estimated with a global fire assimilation system based on observed fire radiative power *Biogeosciences* **9** 527–54

Kong H, Lin J, Chen L, Zhang Y, Yan Y, Liu M, Ni R, Liu Z and Weng H 2022 Considerable unaccounted local sources of NO_x emissions in china revealed from satellite *Environ. Sci. Technol.* **56** 7131–42

Kong H, Lin J, Ni R, Du M, Wang J, Chen L, Xu C, Yan Y, Weng H and Zhang Y 2025 Satellite detected weak decline of nitrogen oxides emissions in economically small cities of China *Environ. Res. Lett.* **20** 074046

Li J F and Wang Y H 2019 Inferring the anthropogenic NO_x emission trend over the United States during 2003–2017 from satellite observations: was there a flattening of the emission trend after the Great Recession? *Atmos. Chem. Phys.* **19** 15339–52

Li M, Liu H, Geng G, Hong C, Liu F, Song Y and He K 2017 Anthropogenic emission inventories in China: a review *Natl Sci. Rev.* **4** 834–66

Liu F, Beirle S, Zhang Q, Dörner S, He K and Wagner T 2016 NO_x lifetimes and emissions of cities and power plants in polluted background estimated by satellite observations *Atmos. Chem. Phys.* **16** 5283–98

Liu F, Beirle S, Zhang Q, van der A R J, Zheng B, Tong D and He K 2017 NO_x emission trends over Chinese cities estimated from OMI observations during 2005–2015 *Atmos. Chem. Phys.* **17** 9261–75

Liu F, Zhang Q, Tong D, Zheng B, Li M, Huo H and He K B 2015 High-resolution inventory of technologies, activities, and emissions of coal-fired power plants in China from 1990 to 2010 *Atmos. Chem. Phys.* **15** 13299–317

Liu M *et al* 2019a Improved aerosol correction for OMI tropospheric NO_2 retrieval over East Asia: constraint from CALIOP aerosol vertical profile *Atmos. Meas. Tech.* **12** 1–21

Liu M *et al* 2020 A new TROPOMI product for tropospheric NO_2 columns over East Asia with explicit aerosol corrections *Atmos. Meas. Tech.* **13** 4247–59

Liu S *et al* 2024 Underappreciated emission spikes from power plants during heatwaves observed from space: case studies in India and China *Earth's Future* **12** e2023EF003937

Liu X *et al* 2019b Updated hourly emissions factors for chinese power plants showing the impact of widespread ultralow emissions technology deployment *Environ. Sci. Technol.* **53** 2570–8

Lu L, Cohen J B, Qin K, Li X and He Q 2025 Identifying missing sources and reducing NO_x emissions uncertainty over China using daily satellite data and a mass-conserving method *Atmos. Chem. Phys.* **25** 2291–309

Murray C J L, Aravkin A Y, Zheng P, Abbafati C, Abbas K M, Abbasi-Kangevari M and Lim S S 2020 Global burden of 87 risk factors in 204 countries and territories, 1990–2019: a systematic analysis for the global burden of disease study 2019 *Lancet* **396** 1223–49

National Bureau of Statistics of China 2024 China Statistical Yearbook 2024 (National Bureau of Statistics of China)

National Development and Reform Commission 2014 Upgrading and retrofitting action plan for energy conservation and pollution mitigation in the coal-fired power sector (available at: www.mee.gov.cn/gkml/hbb/gwy/201409/t20140925_289556.htm) (Accessed 2 August 2025)

Seinfeld J H, Pandis S N and Noone K 1998 Atmospheric chemistry and physics: from air pollution to climate change *Phys. Today* **51** 88–90

State Council of China 2013 The action plan for air pollution prevention and control (available at:

www.gov.cn/gongbao/content/2013/content_2496394.htm) (Accessed 12 December 2025)

State Council of China 2017 13th five-year plan for energy saving and emission reduction (available at: www.gov.cn/gongbao/content/2017/content_5163448.htm) (Accessed 12 December 2025)

Tang L *et al* 2019 Substantial emission reductions from Chinese power plants after the introduction of ultra-low emissions standards *Nat. Energy* **4** 929–38

Tong D *et al* 2018 Current emissions and future mitigation pathways of coal-fired power plants in China from 2010 to 2030 *Environ. Sci. Technol.* **52** 12905–14

Wang M, Li R, Zhang M, Chen L, Zhang F and Huang C 2023 Mapping high-resolution energy consumption CO_2 emissions in China by integrating nighttime lights and point source locations *Sci. Total Environ.* **900** 165829

Weng H, Lin J, Martin R, Millet D B, Jaeglé L, Ridley D, Keller C, Li C, Du M and Meng J 2020 Global high-resolution emissions of soil NO_x, sea salt aerosols, and biogenic volatile organic compounds *Sci. Data* **7** 148

Xu T Y, Zhang C X, Xue J K, Hu Q H, Xing C Z and Liu C 2023 Estimating hourly nitrogen oxide emissions over East Asia from geostationary satellite measurements *Environ. Sci. Technol. Lett.* **11** 122–9

Yan X, Xu Y and Pan G 2023 Evolution of China's NO_x emission control strategy during 2005∼2020 over coal-fired power plants: a satellite-based assessment *J. Environ. Manage.* **348** 119243

Zeng M, Tao M, Li R, Ma P, Zhang L, Wang J, Wang L, Wang Y, Huang H and Chen L 2025 Tracking NO_2 and CO pollution hotspots at provincial scale in China with TROPOMI observations and image segmentation method *Atmos. Environ.* **351** 121176

Zhang Y, Lin J, Liu M, Kong H, Chen L, Weng H and Li C 2022 High-resolution tropospheric NO_2 retrieval over Asia based on OMI POMINO v2.1 and quantitative comparison with other products *Natl Remote Sens. Bull.* **26** 971–87

Zhang Y *et al* 2025 Global retrieval of TROPOMI tropospheric HCHO and NO_2 columns with improved consistency based on the updated Peking University OMI NO_2 algorithm *Atmos. Meas. Tech.* **18** 1561–89

Zheng B *et al* 2018 Trends in China's anthropogenic emissions since 2010 as the consequence of clean air actions *Atmos. Chem. Phys.* **18** 14095–111

Zhu J, Chen L and Liao H 2022 Multi-pollutant air pollution and associated health risks in China from 2014 to 2020 *Atmos. Environ.* **268** 118829